Chains of gold atoms with tailored electronic states

J. N. Crain,[1] J. L. McChesney,[1] Fan Zheng,[1] M. C. Gallagher,[2] P. C. Snijders,[3] M. Bissen,[4] C. Gundelach,[4] S. C. Erwin,[5] and F. J. Himpsel[1]

[1]*Department of Physics, University of Wisconsin-Madison, 1150 University Avenue, Madison, Wisconsin 53706, USA*

[2]*Department of Physics, Lakehead University, Thunder Bay, Ontario P7B 5E1, Canada*

[3]*Department of NanoScience, Delft University of Technology, Lorentzweg, 2628 CJ Delft, The Netherlands*

[4]*Synchrotron Radiation Center, University of Wisconsin-Madison, 3731 Schneider Drive, Stoughton, Wisconsin 53589, USA*

[5]*Center for Computational Materials Science, Naval Research Laboratory, Washington, DC 20375, USA*

(Received 11 August 2003; published 5 March 2004)

A combination of angle-resolved photoemission and scanning tunneling microscopy is used to explore the possibilities for tailoring the electronic structure of gold atom chains on silicon surfaces. It is shown that the interchain coupling and the band filling can be adjusted systematically by varying the step spacing via the tilt angle from Si(111). Planes with odd Miller indices are stabilized by chains of gold atoms. Metallic bands and Fermi surfaces are observed. These findings suggest that atomic chains at stepped semiconductor substrates make a highly flexible class of solids approaching the one-dimensional limit.

DOI: 10.1103/PhysRevB.69.125401 PACS number(s): 73.20.At, 71.10.Pm, 79.60.Jv, 81.07.Vb

MOTIVATION

It has been predicted for some time that electrons exhibit fundamentally different properties when confined to move along a single dimension.[1] Single-particle excitations are replaced by collective excitations since the wave functions overlap strongly and become highly correlated. This collectivization has startling consequences on the physics of one-dimensional systems leading to a variety of unusual phases at low temperatures.[2–5] In a one-dimensional metal even the identity of individual electrons is lost, instead replaced by separate spin and charge excitations.[3]

The theory of correlated electron phases has opened up a new field of electron physics in one dimension that has led to a steadily increasing library of predictions for novel electron behavior. While the predictions give glimpses of exotic physics, finding direct evidence for spin-charge separation has proven elusive. The key difficulty lies in engineering one-dimensional systems with controlled electronic properties. For example, metallic systems with 1/2-filled bands become unstable in one dimension due to a Peierls distortion. Among the few exceptions are carbon nanotubes. They need to be measured individually in order to select a tube with a specific diameter and chirality. That limits the applicable probing techniques to microscopic methods. Here we explore a complementary approach, where a macroscopic array of atomic chains is created at a surface by self-assembly. These structures are robust compared to other classes of quasi-one-dimensional materials, such as organic charge transfer salts or transition metal chalcogenides, and they can be fabricated easily over large areas. Such a structure is ideally matched to photoemission as a probing method, which is unique in being able to measure the complete set of quantum numbers of an electron in a solid: i.e., energy, momentum, spin, and point group symmetry.[6,7]

Silicon is chosen as a substrate for the formation of chain structures for several reasons. The band gap of silicon prevents metallic states at the Fermi surface from coupling to the substrate both in two dimensions[8,9] and in one dimension.[10,11] The Si(111) surface and its vicinal surfaces (see Fig. 1) exhibit a natural tendency to form anisotropic reconstructions of metal atoms at the surface. Already the flat Si(111) surface breaks its threefold symmetry at submonolayer coverage and forms three domains of anisotropic $n \times 1$ structures for many metals.[12] Furthermore, the use of stepped silicon[13] introduces an additional anisotropy at the surface that drives the formation of one-dimensional chain structures parallel to the step direction, which is $[1\,\bar{1}\,0]$ in our case. With gold atoms the ideal limit of a single chain per terrace can be achieved.[11,12,14–21] We find that most of these self-assembled gold chains on silicon display metallic states.

Exploring electron behavior in one dimension requires the tailoring of the parameters that determine the electronic phase diagram. One of the key parameters for metallic states is the band filling. The size of the spin-charge separation effect is determined critically by the strength of the electron-electron interaction U, but for U greater than the bandwidth W a $\frac{1}{2}$-filled band undergoes a Mott-Hubbard transition to an insulator, precluding the observation of a metallic Luttinger liquid. Changing the filling from $\frac{1}{2}$ to $\frac{1}{4}$ and other fractional fillings may maintain the metallicity of a band even in the presence of strong interactions.[11,22] An equally important parameter for fabricating one-dimensional systems is the two-dimensional coupling strength between adjacent chains, since exotic physics is predicted only in the limit of small coupling.

In the present work we demonstrate the capability of tailoring one-dimensional electronic states for chains of gold atoms on stepped silicon surfaces. By tuning the tilt angle of the surface from (111) and the gold coverage, chains with variable spacing are obtained. The band dispersions and Fermi surfaces for these chains are measured via angle-resolved photoemission and analyzed in the framework of normal electron bands, a treatment which seems appropriate

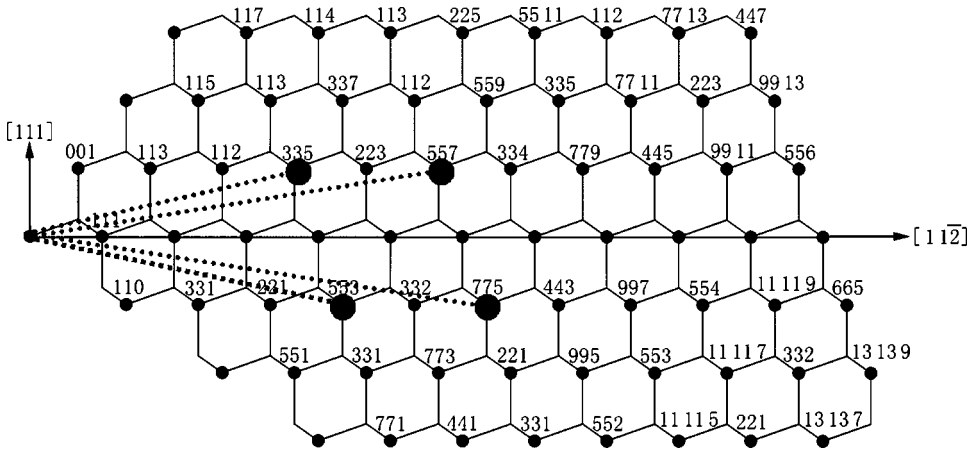

FIG. 1. Side cutaway showing the crystal lattice of silicon in the $(1\ \bar{1}\ 0)$ plane, which is perpendicular to the steps and to the (111) surface. Vicinal surfaces tilted from $[1\ 1\ 1]$ towards both $[\bar{1}\ \bar{1}\ 2]$ and $[1\ 1\ \bar{2}]$ form a series of stable step structures with Au. The dotted lines show the cross section of the four vicinal surfaces discussed here. The flat Si(111) surface corresponds to a horizontal line (the x axis).

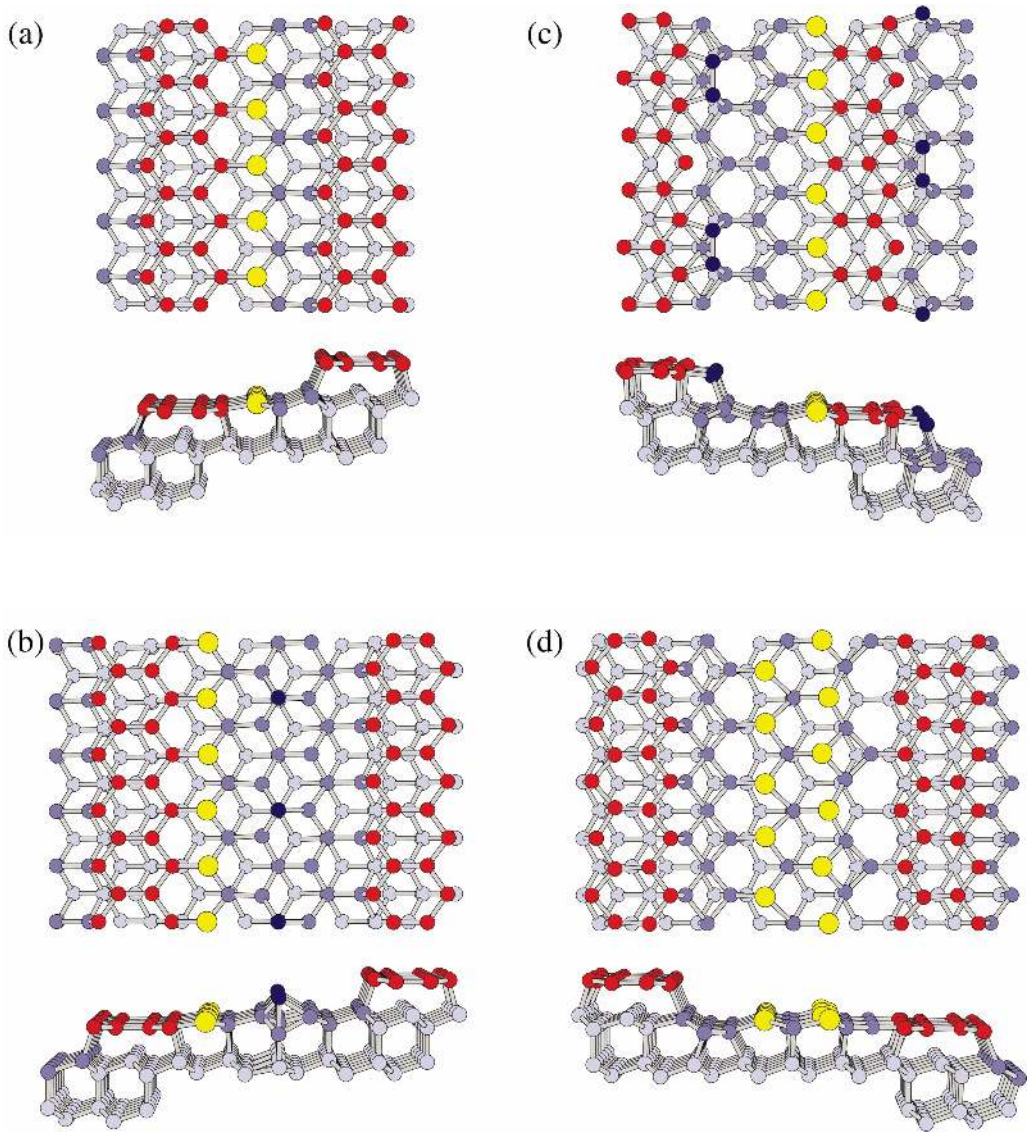

FIG. 2. (Color) Structural models (Ref. 34) for prototypical gold chain structures on stepped Si(111). (a) Si(335)-Au, (b) Si(557)-Au, (c) Si(553)-Au, and (d) Si(775)-Au.

down to energy scales of 0.1 eV. Exotic correlated states, such as spinons and holons, are likely to become relevant at an energy scale of meV, judging from the energy scale of such states in two-dimensional systems. These chains exhibit a range of band fillings and interchain couplings, which are determined directly from the photoemission data. The aim of this work is the systematic exploration of the options for varying these parameters. Exploiting the largest possible parameter space may hold the key to observing exotic physics in one dimension, including spin-charge separation, which likely will be found at smaller energy scales.

STRUCTURE OF GOLD CHAINS ON STEPPED Si(111)

Already on flat Si(111) the deposition of gold leads to an anisotropic 5×2 chain reconstruction.[10,14,23,24] Similar $n\times1$ and $n\times2$ reconstructions are formed by deposition of silver,[25] alkali metals,[26,27] alkaline earths,[26,27] and rare earths.[28] However, for flat substrates the length of the chains is limited due to the domain structure imposed by the threefold symmetry of the underlying lattice, which allows three equivalent chain directions ($[1\,\bar{1}\,0]$, $[0\,1\,\bar{1}]$, $[\bar{1}\,0\,1]$). Stepped silicon surfaces break the threefold symmetry of the substrate and lead to a single domain if the step edge is chosen along one of the three equivalent chain directions. Stepped Si(111) templates have been prepared with high perfection by appropriate annealing sequences.[29–31] At low enough coverage there is only a single gold chain in the unit cell of such vicinal surfaces, while the flat Si(111)5 $\times2$-Au structure consists of two Au chains per unit cell.[32]

Figure 1 shows how vicinal Si(111) surfaces containing the stable $[1\,\bar{1}\,0]$ steps can be classified into two groups, one tilted with its normal towards the $[1\,1\,\bar{2}]$ azimuth with one broken bond at the step edge, the other towards $[\bar{1}\,\bar{1}\,2]$ with two broken bonds. Consider a cut through the silicon crystal structure perpendicular to the steps. Various vicinal surfaces intersect the plane of the drawing along the dotted lines. All possible vicinal surfaces begin at the origin (the leftmost lattice point) and end at an equivalent lattice point labeled with the Miller index of the corresponding vicinal surface [for example, (335), (557), (553), (775) for surfaces studied in detail here]. The two groups of vicinal surfaces have end points above and below this line, and their normal is tilted from the [111] direction towards $[\bar{1}\,\bar{1}\,2]$ and $[1\,1\,\bar{2}]$, respectively. The overall electron count is the same, odd for the bare Si surface and even after adding one electron from the Au chain. The diagram in Fig. 1 yields an infinite number of combinations, where the step spacing can be varied in units of 0.22 nm (2/3 of the lattice constant along the $[\bar{1}\,\bar{1}\,2]$ direction).

Here we select four prototypical orientations, which allow us to systematically study the dependence of the electronic structure on the step spacing for both classes of vicinal surfaces. They begin with the smallest chain spacing that exhibits the desired Au chain structure: i.e., (335) and (553). The nominal step spacing would be even smaller for (113) and (331), but they form facets with other orientations.[33] Surfaces with mixed even and odd indices (to be multiplied by 2 for true Miller indices) do not form useful chain structures. The four selected surfaces can be thought of as a series of Si(1 1 1) terraces separated by single silicon steps. The resulting unit cells incorporate atoms from the step edge as part of the reconstruction. The unit cells of Si(335)-Au and Si(553)-Au in Fig. 2 consist of single terraces 3-2/3 and 4-1/3 silicon rows wide, plus a single step. Si(557)-Au and Si(775)-Au contain 5-2/3 and 6-1/3 silicon rows, respectively. These terrace widths determine the interchain spacings for the four structures which range from 1.26 nm for (335) up to 2.13 nm for (775). Additional chain structures will be described briefly at the end.

TABLE I. Summary of chain spacings, gold coverages, and tilt angles from [1 1 1] for several gold chain structures on vicinal silicon surfaces. The coverages are in units of Si(111) monolayers (ML).

Orientation	Spacing (nm)	Au coverage (ML)	Off-axis angle
Si(111)5×2-Au	1.67	0.4	0°
Si(335)-Au	1.26	0.27 ± 0.04	14.4° to $[\bar{1}\,\bar{1}\,2]$
Si(557)-Au	1.92	0.18 ± 0.04	9.5° to $[\bar{1}\,\bar{1}\,2]$
Si(553)-Au	1.48	0.24 ± 0.04	12.5° to $[1\,1\,\bar{2}]$
Si(775)-Au	2.13	0.25 ± 0.07	8.5° to $[1\,1\,\bar{2}]$
Si(995)-Au	2.63	0.13 ± 0.04	13.8° to $[1\,1\,\bar{2}]$
Si(13 13 7)-Au	3.78	0.09 ± 0.04	14.4° to $[1\,1\,\bar{2}]$
Si(110)5×2-Au	2.72	0.30 ± 0.07	35.3° to $[1\,1\,\bar{2}]$

Figure 2 shows our most promising (but not yet final) structural models of the four orientations studied here. The models were arrived at through a combination of first-principles total-energy calculations,[16,34] x-ray diffraction,[18] calculated versus measured band structures,[34] and scanning tunneling microscope (STM) images. In the following we outline our basic approach to constructing the models and summarize the results of our total-energy calculations. A more detailed description can be found elsewhere.[34]

The total-energy calculations were performed in a slab geometry with up to six layers of Si plus the reconstructed surface layer; all atomic positions were relaxed except for the bottom layer, which was passivated. Total energies and forces were calculated within the local-density approximation to density-functional theory, using ultrasoft pseudopotentials and a plane-wave basis.[35,36] To establish first the basic features of Au adsorption, we investigated the energetics of an isolated Au adsorbate on a flat, unreconstructed Si(111) surface. For this model system, the Au atom very strongly prefers to substitute into the top Si layer: for example, the energy gained relative to adsorption above the surface is 1.7 eV. Substitution in the top Si layer is also more favorable than in the second layer, by 1.4 eV. Such large energy differences strongly suggest that Au will invariably prefer to occupy a substitutional site in the topmost Si layer, and hence all of our models reflect this.

The remaining details of the individual models were elucidated in different ways. For Si(553)-Au, more than 40 structural models were studied with total-energy calcula-

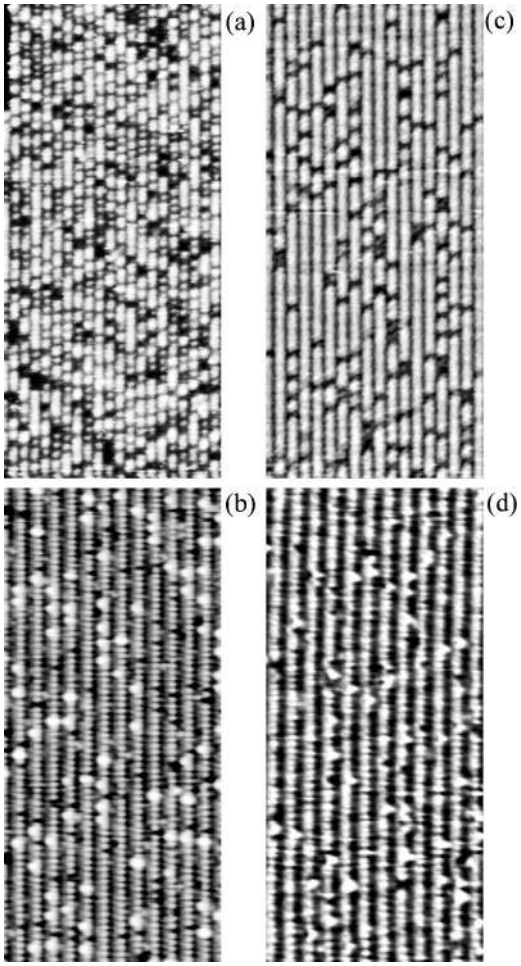

FIG. 3. Images of four chain structures of gold on silicon: (a) Si(335)-Au, (b) Si(557)-Au, (c) Si(553)-Au, and (d) Si(775)-Au. In addition to atomic chains there are point defects which play a role in doping the chains. They appear as dark voids for small chain spacing (a), (c) and as bright protrusions for large spacing (b), (d). 25×55 nm^2 STM images, filled states at -1 V sample bias for (a), (c), and empty states at $+2$ V for (b), (d).

tions. The model shown in Fig. 2 has the lowest surface energy of those considered. It is degenerate, within our estimated precision, with six other models that mainly differ in the details of the step-edge reconstruction. The model shown here agrees best with the 1×3 reconstruction seen by STM and with the 8/3 electron count determined from the Fermi surface. For Si(557)-Au, similar studies were carried out for about 25 structural models. The model shown has the lowest surface energy. It is similar to a model proposed by Sanchez-Portal *et al.*[16] (see also Ref. 37), but with the addition of Si adatoms in T_4 surface sites [dark blue in Fig. 2(b)], as suggested by x-ray diffraction.[18] We find that these adatoms indeed lower the energy slightly. For Si(335)-Au and Si(775)-Au, no explicit calculations were performed, and the models shown here simply represent analogs of other surfaces. The model shown for Si(775)-Au is a simple transfer of a structure proposed recently[38] for flat Si(111)5×2-Au onto a terrace, and the model for Si(335)-Au is a truncation of the Si(557)-Au structure.

The energetically favorable models for both the Si(553)-Au and Si(557)-Au often contain a group of nearly planar π-bonded Si atoms which may be viewed as a strip of graphitic Si atoms. This π bonding, like the π-bonded 2×1 chain reconstruction of cleaved Si(111),[39] significantly reduces the surface energy on Si(111). This structural element appears in our (335), (557), and (775) models as the common ''honeycomb chain'' subunit shown in red. This feature is well established as an elementary building block of the alkali-induced 3×1 reconstruction of Si(111).[26] Its reappearance in our models for Au-induced reconstructions is therefore, we believe, a plausible possibility. Note that in these vicinal orientations the Si honeycomb generally appears at the step edge and hence may be a viable alternative to step rebonding, reconstruction, or decoration.

A special feature of the Si(553)-Au structure, and possibly the other structures, too, consists of extra Si atoms attached to the step edge [dark blue in Fig. 2(c)]. There are many possible arrangements with similar energies (1×2, 1×3, monomers, dimers, different sites). These might be responsible for mobile Si atoms at the step edges that form 1×2

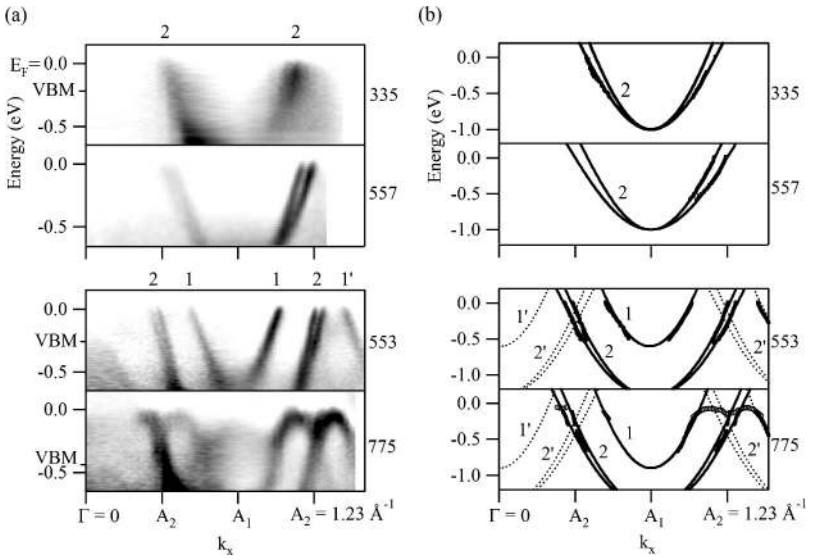

FIG. 4. Band dispersions in the chain direction k_x for two pairs of Au chain structures on stepped Si(111): Si(335)-Au, Si(557)-Au, Si(553)-Au, and Si(775)-Au. The upper pair exhibits a doublet of nearly half-filled bands (labeled 2), the lower pair an additional quarter-filled band (labeled 1). The bottom of all bands lies at the one-dimensional Brillouin zone boundary A_1, while the region near the zone center Γ (left) lacks surface states due to the presence of bulk bands. Backfolded bands due to period doubling along the chain are indicated by dotted lines and primed labels.

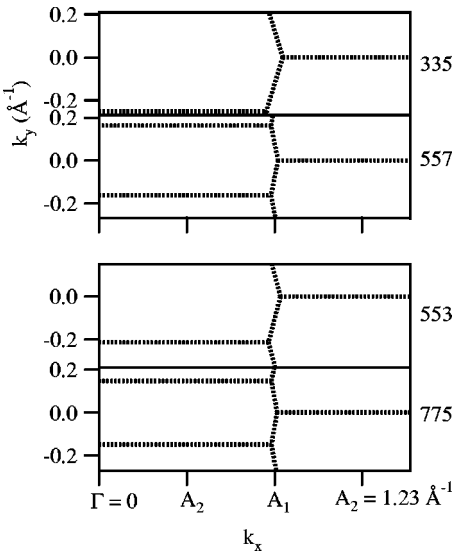

FIG. 5. Brillouin zones for the four Au chain structures (neglecting superlattice formation). Increased chain spacing makes the Brillouin zone narrower in the direction perpendicular to the chains (k_y), such that the zigzag zone boundary straddling the A_1 point approaches a truly one-dimensional line. A_2 corresponds to the zone boundary after doubling the period along the chain.

and 1×3 superlattices when pinned by defects [see a close-up STM image of Si(553)-Au in Ref. 11]. They are also responsible for doping the chains and creating a fractional electron count of 8/3 in Si(553)-Au (see below).

The Au chains are affected very little by period doubling and tripling in other parts of the unit cell. Their positions are locked in by three backbonds to the Si substrate. There is no evidence for dimerization of the Au atoms from either x-ray diffraction, which is sensitive to heavy atoms,[18] or from total-energy calculations, which favor symmetric lattice positions, not dimers.[34] The only exceptions are Si(111)5 $\times2$-Au and Si(775)-Au, which contain two Au chains per unit cell with a left-right buckling in Fig. 2(d).

FABRICATION OF Au CHAINS

Gold chains are produced by self-assembly on Si using a straightforward deposition and annealing sequence. First, clean silicon surfaces are prepared using a previously optimized heating sequence[31] that produces straight, regularly spaced steps on vicinal silicon wafers. Next, the appropriate gold coverage (see Table I) is deposited with the surface at an elevated temperature of 650 °C. Optimum long-range order is achieved via a final flash to 850 °C for a few seconds followed by slow cooling over several minutes. The deposition of gold strongly rearranges the vicinal surfaces, e.g., by breaking up triple steps[40] on clean Si(557) into single steps on Si(557)-Au. The optimum coverage is a single gold atom per unit cell for Si(335)-Au,[17] Si(557)-Au,[15,18,19,41] and Si(553)-Au.[11] Si(775)-Au requires more gold, almost two atoms per unit cell, similar to the two gold chains for Si(111)-5$\times2$-Au.

Figure 3 compares STM images for the four related chain structures of gold on silicon: Si(335)-Au, Si(557)-Au, Si(553)-Au, and Si(775)-Au. They exhibit long atomic chains with the chain spacing ranging from 1.26 to 2.13 nm between the different step structures (Table I). The chains extend over long distances (hundreds of nm), only interrupted by occasional steps crossing the chains due to a slight azimuthal misorientation of the surface (not shown).

The perfection of the chains is mainly limited by point defects, which appear either as dark voids [for the two surfaces with small chain spacing, Si(553)-Au and Si(335)-Au] or as bright protrusions [for the two surfaces with large chain spacing, Si(775)-Au and Si(557)-Au]. Their density is inversely correlated with the momentum width of the electronic states in photoemission. Si(335)-Au has the highest defect density, Si(553)-Au the lowest. Correspondingly, the momentum distributions in photoemission are sharpest for Si(553)-Au and broadest for Si(335)-Au. There is some evidence that the defects influence the electronic structure by doping the chains. For example, a 1×3 ordering of voids in Si(553)-Au is able to explain a fractional electron count of 8/3 electrons per Au atom by having two extra Si atoms in the unit cell.[11] On Si(111)5$\times2$-Au a half-filled 5×4 lattice of extra Si atoms provides just the right band filling for the structure with the lowest total energy.[23,38]

The optimum tunneling conditions were found at positive sample bias (empty states) in the case of Si(557)-Au and Si(775)-Au and at negative bias (filled states) for the other two structures. Both empty- and filled-state images of Si(557)-Au and Si(775)-Au show chains with a doubled 1×2 period. The void structures on the other two structures tend to order into a tripled 1×3 periodicity. An additional weak 1×2 periodicity appears in the valleys between the chains for Si(553)-Au (for a detailed STM image see Ref. 11). In order to identify the chains seen in the STM images we compare them to the structural models in Fig. 2. The atoms visible to STM are most likely not Au chain atoms, but Si atoms with broken bonds, such as the Si adatoms for Si(557)-Au [dark blue in Fig. 2(b)] and the Si atoms at the step edge. The Au atoms are more electronegative than Si and bind one Si electron with their *s,p* electrons in a low-lying state[16] that is not visible in STM.

BAND DISPERSIONS

$E(k_x,k_y)$ band dispersions were obtained using a Scienta 200 spectrometer with E, ϑ multidetection using *p*-polarized synchrotron radiation at $h\nu=34$ eV, where the cross section of the surface states peaks (for details see Refs. 9 and 14). Figure 4 displays the band dispersion $E(k_x)$ along the chain direction for all four chain structures. The photoemission intensity is plotted in a gray scale with high intensity shown dark. A shallow high-pass filter eliminates slow intensity variations and makes the $E(k)$ relation better visible. These data are for a sample temperature of <100 K [150 K for Si(557)-Au], colder than our previously published measurements on the Si(557)-Au and Si(553)-Au surfaces.[11,15] The band dispersions in Fig. 4 are given with respect to the Fermi level E_F and the position of the valence-band maximum (VBM) of Si indicated as well. It was obtained from Si $2p$ core-level data taken together with the valence-band results

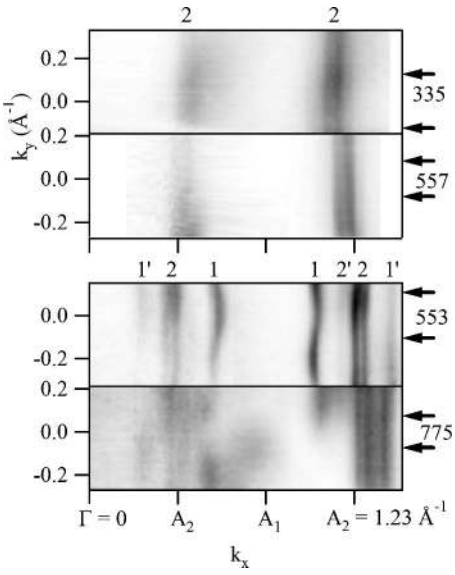

FIG. 6. Fermi surfaces of the four Au chain structures: Si(335)-Au, Si(557)-Au, Si(553)-Au, and Si(775)-Au (at $E_F-0.1$ eV). The corresponding portions of the Brillouin zone are shown in Fig. 5. High photoemission intensity is dark. The Fermi surface of a one-dimensional structure consists of vertical lines (Fermi points along k_x spread out into lines along k_y). Small undulations in these lines indicate weak two-dimensional coupling. The labels refer to the corresponding bands in Fig. 4 (2 for the doublet of nearly half-filled bands, **1** for the quarter-filled band, and **2**′,**1**′ for replicas from back-folding at the point of half filling A_2).

(for the method see Ref. 42 and 43). At low temperatures there is a substantial photovoltage, particularly with *n*-type samples, which makes an absolute determination of the Fermi level uncertain by about 50 meV. Therefore, we can only say that these surfaces are metallic within the uncertainty of the Fermi level determination, possibly larger for the semimetallic Si(775)-Au surface.

Si(553)-Au exhibits three metallic bands that disperse along the chain direction k_x, all with minima at the Brillouin zone boundary of the 1×1 unit cell (A_1 in Fig. 5). These are a single upper band (labeled **1**) and a close pair of lower bands (labeled **2**). Interestingly, all of the bands observed for the four different structures appear to be a subset of these three. The direction of the tilt angle with respect to (111) plays a key role in determining the band structure. The two surfaces that are tilted towards $[\bar{1}\bar{1}2]$, Si(335)-Au and Si(557)-Au, display only band **2**, while the two surfaces tilted towards $[11\bar{2}]$, Si(553)-Au and Si(775)-Au, display both the inner band **1** and the outer doublet **2**. The cross section of the metallic bands versus photon energy is similar to that of silicon broken-bond states, which peaks at $h\nu=34$ eV relative to that of the bulk bands.[14] This leads us to assign the metallic bands to rows of silicon broken bonds—for example, those at the step edges or those pointing towards the gold atoms. This would be compatible with the electronegativity argument given above.

Weak additional bands **1**′ and **2**′ are observed for Si(775)-Au and Si(553)-Au that correspond to a backfolding of bands of **1** and **2** at the 1×2 zone boundary A_2. In the case of Si(553)-Au a duplicate **1**′ of **1** is visible in the second Brillouin zone at the far right of Fig. 4, shifted by a 1×2 reciprocal lattice vector. In the case of Si(775) the band structure is nearly symmetric about A_2, showing backfolded versions of both **1** and **2**. Such backfolding suggests period doubling along the chains accompanied by a small band gap at the new zone boundary A_2. Such gaps are not resolved here, but a recent study of Si(557)-Au finds indeed temperature-dependent gaps at this point,[21] even though backfolding has not been observed yet for this surface. Doubled periods are seen in STM for many of these surfaces. Not all of them are directly related to the Au chains, such as the Si adatoms on Si(557)-Au which create a strong corrugation with doubled period in STM, but affect the Au chains very little [see Fig. 2(b)]. However, the second chain in Si(557)-Au which corresponds to the step edge has been observed to dimerize at low temperatures where the gap opens.[21] For Si(553)-Au there is a weak double period in the valleys between the bright single-period chains, mostly adjacent to 1×3 pinning centers [not shown; see Ref. 11, Fig. 3(d) for a high-resolution image]. For Si(775)-Au one expects strong backfolding due to the left-right buckling of the two Au chains [Fig. 2(d)].

Precise $E(k_x)$ band dispersions are obtained by fitting Lorentzians to the individual momentum distribution curves (MDC's) taken from the left panels of Fig. 4. The resulting peak positions are plotted in the panels on the right side of Fig. 4 as solid circles. In the case of Si(775)-Au the flatness of the bands in the vicinity of the Fermi surface makes fitting to MDC's inaccurate and thus peak positions are determined using energy distribution curves (EDC's), shown as open circles. To quantify the band parameters for each surface the data are modeled by a tight-binding calculation with three coupling parameters: t_1 and t_3 for the first and second neighbors along the chains (at $x=\pm a$, $x=\pm2a$) and t_2 for the first neighbors in the adjacent chains (at $x=\pm1/2$, $y=$

TABLE II. Band parameters calculated from the $E(k_x)$ band dispersions and Fermi surfaces for Au chains on stepped Si(1 1 1). The bandwidth is $W_x=4t_1$ along k_x. The bottom of the band is $E_{\min}=E_0-2t_1+2t_3$. The effective masses range from 0.3 to 0.65. The band filling is given by $\langle k_F\rangle/(\pi/a)$, with a filling of 1 corresponding to two electrons per chain atom.

Band		Filling	E_0 [eV]	t_1 [eV]	t_3 [eV]	t_2 [eV]
Si(335)-Au	**2**	0.38	0.7	0.85		0.05
	2	0.43	0.32	0.66		0.04
Si(557)-Au	**2**	0.42	0.36	0.68	<0.02	<0.01
	2	0.49	0.04	0.54	<0.02	<0.01
Si(553)-Au	**1**	0.27	1.28	0.96	<0.03	0.08
	2	0.51	0.04	0.73	0.065	0.016
	2	0.56[a]	−0.16	0.63	0.065	0.016
Si(775)-Au[b]	**1**	b	0.98	0.96	<0.03	~0.02
	2	b	−0.11	0.73	0.065	<0.007
	2	b	−0.31	0.63	0.065	<0.006

[a]This value corrects an earlier typographic in Ref. 11. See Ref. 45.
[b]The flat bands near E_F are nearly filled, suggesting a semi metallic band structure with just the band maxima touching the Fermi level.

$\pm b$). The constants a and b are the atomic spacings along and between the chains. The resulting band dispersion and Fermi surface are given by

$$\begin{aligned} E(k_x,k_y) &= E_0 + t_1[\exp(ik_x a) + \exp(-ik_x a)] \\ &\quad + t_3[\exp(ik_x 2a) + \exp(-ik_x 2a)] \\ &\quad + \tfrac{1}{2}t_2\{\exp[i(k_x a/2 + k_y b)] \\ &\quad + \exp[i(k_x a/2 - k_y b)] \\ &\quad + \exp[i(-k_x a/2 + k_y b)] \\ &\quad + \exp[i(-k_x a/2 - k_y b)]\} \\ &= E_0 + 2[t_1 \cos(k_x a) + t_3 \cos(2k_x a) \\ &\quad + t_2 \cos(k_x a/2)\cos(k_y b)] \end{aligned}$$

and

$$\begin{aligned} k_y(k_x) = b^{-1} \arccos\{&[\tfrac{1}{2}(E_F - E_0) - t_1 \cos(k_x a) \\ &- t_3 \cos(2k_x a)]/t_2 \cos(k_x a/2)\} \end{aligned}$$

(Ref. 11) (for a basic introduction to the tight-binding model see Ref. 44). For Si(553)-Au the band parameters have been determined previously.[11] For Si(775)-Au bands **1** and **2** are modeled by using the fits for Si(553)-Au and shifting them by -0.3 and -0.15 eV, respectively.

FERMI SURFACES AND DIMENSIONALITY

Figure 6 shows the Fermi surfaces of the three metallic chain structures [Si(335)-Au, Si(557)-Au, Si(553)-Au] and an energy surface at $E_F - 0.1$ eV for Si(775)-Au where bands **1** and **2** are clearly resolvable. Si(775)-Au exhibits very flat bands near the Fermi level that touch E_F with their maxima and give rise to semimetallic Fermi points. These occur near $A_2 \pm g_x/16$ where $g_x = 2\Gamma A_1$ is the reciprocal lattice vector along x. The regions of the Brillouin zone covered by each of the panels in Fig. 6 are identical to the corresponding panels in Fig. 5. The Fermi surfaces in Fig. 6 are labeled the same way as the bands in Fig. 4 to facilitate the comparison.

At a first glance the constant energy surfaces are close to the expectation for a one-dimensional system—i.e., Fermi points stretched out into straight lines along k_y (perpendicular to the chains). Upon closer inspection some of these Fermi lines exhibit oscillations which correspond to a weak two-dimensional coupling between the chains. A fully two-dimensional Fermi surface tends to become a closed curve, such as the Fermi circle of a free electron and the circles observed[9] for two-dimensional $\sqrt{3}\times\sqrt{3}$ and $\sqrt{21}\times\sqrt{21}$ structures of Au and Ag on Si(111). The deviation of the Fermi surfaces from straight lines increases for smaller chain spacings [Si(335)-Au and Si(553)-Au], as expected from the better overlap between the wave functions.

To quantify the two-dimensional coupling we use again fits to MDC's, such as those shown in Figs. 7 and 8. The amplitude of these oscillations defines the interchain coupling strength t_2 in a tight-binding model,[11] and the resulting coupling strengths are tabulated in Table II for each of the

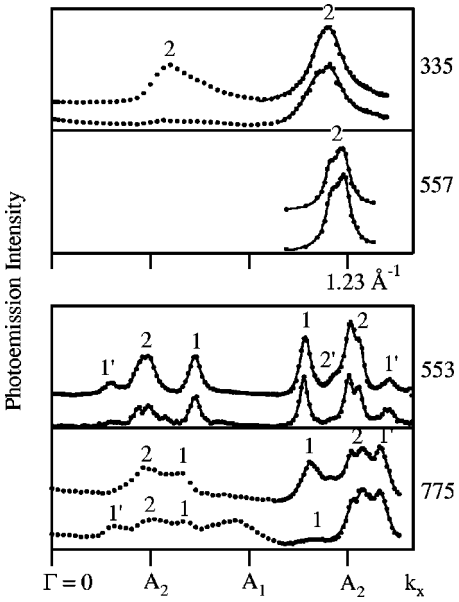

FIG. 7. Quantitative evaluation of the Fermi surface and band filling via momentum distribution curves (MDC's) along the chain direction k_x. From top to bottom, Si(335)-Au, Si(557)-Au, Si(553)-Au (all at E_F), and Si(775)-Au (at $E_F - 0.1$ eV). k_y is fixed at $\pm\pi/2b$ (upper/lower curves), the average points of the k_y dispersion (marked by arrows in Fig. 6). The peaks are labeled the same way as in Figs. 4 and 6.

structures. This two-dimensional coupling can be compared to the one-dimensional coupling along the chains t_1 and their ratio quantifies the dimensionality of the bands. For the double band **2** we obtain $t_1/t_2 = 17$ in Si(335)-Au, $t_1/t_2 = 46{,}39$ in Si(553)-Au, $t_1/t_2 > 60$ for Si(557)-Au, and $t_1/t_2 > 100$ for Si(775)-Au, where no oscillations are detectable within our detection limit of ± 0.002 Å^{-1}. Band **1** also exhibits oscillations that are particularly strong for Si(553)-Au, resulting in a ratio $t_1/t_2 = 12$. As one might expect from the wave function overlap, the strength of the interchain coupling depends critically on the distance between the chains and decreases radically for larger spacings. However, with the chain spacing fixed, not every band has the same dimensionality. The individual character of the wave function does matter. The results demonstrate great flexibility for tuning the dimensionality in these chain structures with a range of at least an order of magnitude. These values can be compared to three-dimensional chain structures, such as the Bechgaard salts where a ratio of $t_1/t_2 \approx 10$ has been reported.[4]

BAND FILLING

Another electronic property that can be tailored in gold chain structures is the band filling. Luttinger's theorem allows a quantitative determination of the band fillings from the area inside the Fermi surface, as long as perturbation theory still holds.[46] The normalization is provided by the area of the Brillouin zone, which corresponds to two electrons (with opposite spins) per band (compare Figs. 5 and 6 which cover the same areas of **k** space). Tight-binding fits to Fermi surfaces are used for an accurate determination of

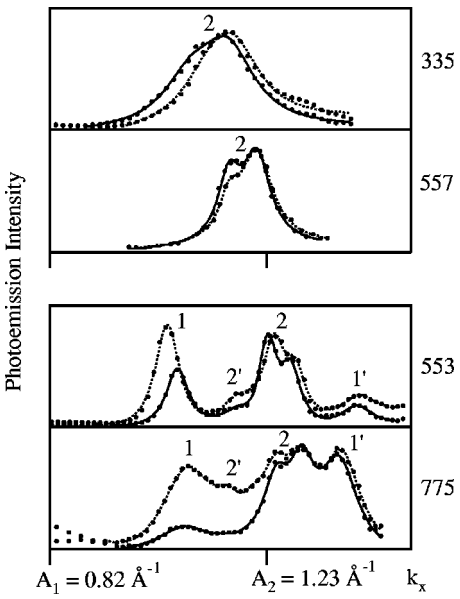

FIG. 8. Perpendicular band dispersion obtained from MDC's in k_x taken at the two external points of the k_y dispersion ($k_y = \pi/b$, 0 = dashed, solid lines). From top to bottom, Si(335)-Au, Si(557)-Au, Si(553)-Au (all at E_F), and Si(775)-Au (at $E_F - 0.1$ eV). A weak two-dimensional dispersion is observed for state **2** in Si(335)-Au and for states **1** and **2** in Si(553)-Au. This dispersion is absent for state **2** on the surfaces with large chain spacing [Si(557)-Au and Si(775)-Au]. Note that the k_x scale covers only half the range of Fig. 7.

their area. The resulting filling is listed in Table II for band **1** and the two components of band **2**. For Si(775)-Au the Fermi surface degenerates into semimetallic points.

Already a glance at the Fermi surfaces in Fig. 6 reveals a systematic increase in the filling of the common doublet band **2** when going from top to bottom. For Si(335)-Au, both branches cross the Fermi level well inside the A_2 point, which corresponds to half filling. For Si(557)-Au the crossings are just inside the A_2 point with the outer band touching A_2, thereby indication a filling of nearly $\frac{1}{2}$. For Si(553)-Au the two branches lie just outside A_2 and yield a filling somewhat larger than $\frac{1}{2}$. For Si(775) band **2** becomes completely filled if one considers the flat bands near E_F as continuations of this band (see Fig. 4). Even taking it as a separate band using the fit curves on the right of Fig. 4 it is slightly more filled than for the other surfaces. Adding the filling of all bands one obtains a monotonically increasing overall filling of 0.81, 0.91, and 1.34 bands for Si(335)-Au, Si(557)-Au, and Si(553)-Au. The corresponding number of electrons per chain atom is twice as much—i.e., 1.62, 1.82, and 2.68. In the case of Si(557)-Au, our band filling is slightly lower than in Ref. 21. The difference could be due to a different density of extra Si atoms on top of the chains that might act as dopants.[11,38]

Simple electron counting provides a first insight into the experimental band filling. Adding the unpaired *s,p* electrons of a Au atom to the number of broken bonds in an unreconstructed 1×1 unit cell gives an even number of electrons for all four chain structures. Introducing extra Si atoms into a reconstructed unit cell adds four extra valence electrons per Si atom. That does not change the parity of the electron count. Thus the observation of fractional overall electron counts deviating significantly from the nearest even number (=2) cannot be explained by such a simple model. For Si(553)-Au there is an explanation that is based on a tripled unit cell.[11] Adding two extra Si atoms at the step edge [dark blue in Fig. 2(c)] provides $8/3 \approx 2.67$ extra electrons per chain atom, which agrees with the observed count of 2.68 within the experimental accuracy. The other two surfaces are not easily explained in this fashion. Most likely, the many defects in Si(335)-Au act as dopants, and the fewer defects in Si(557)-Au might explain why its electron count is closer to the even number 2. Si(553)-Au is the most perfect of the chain structures we studied and therefore the most straightforward to explain.

The band structure of Si(775)-Au with its almost two gold chains per unit cell is actually quite similar to that of Si(111)5×2-Au (Ref. 14), which contains two complete chains.[47] Both surfaces have a high band filling with extra flat bands near the Fermi level making them almost semimetallic. This prompted us to use a structure similar to Si(111)5×2-Au as a model for the terrace of Si(775)-Au in Fig. 2(d). Interestingly, the Si(111)5×2-Au surface appears to be stabilized by a lattice gas of additional Si atoms that provide the energetically optimal band filling.[31,38] Thus autodoping by built-in defects might be a common phenomenon in these chain structures.

MOMENTUM DISTRIBUTION AT E_F

The states near the Fermi level, which are responsible for the possible formation of exotic low-dimensional states, are analyzed more quantitatively in Figs. 7 and 8. Figure 7 addresses the band filling and Fig. 8 the coupling perpendicular to the chains. Cuts through the Fermi surface are shown along the chain direction k_x, with k_y chosen to eliminate the k_y dispersion in Fig. 7 and to maximize it in Fig. 8. Thus both cuts in Fig. 7 should exhibit the same peaks and a consistency check between the two curves eliminates spurious features, such as a variable background or cross section changes in **k** space. In contrast, Fig. 8 shows MDC's with k_y values located half way between the cuts of Fig. 7 which represent the points with maximum k_y dispersion. A shift between the dashed and full curves is a measure of the perpendicular coupling t_2. It is visible for the two structures with the closer chains, Si(335)-Au and Si(553)-Au. These MDC's also confirm the doublet character of band **2** for Si(335)-Au and Si(775)-Au which is difficult to see in the grayscale images. For Si(335)-Au the second component appears only as a shoulder, but it is verified by Lorentzian χ^2 fits.

Backfolded bands become visible for both Si(553)-Au and Si(775)-Au and provide quantitative evidence for a period doubling. These additional peaks, labeled **1′** and **2′**, are symmetric to peaks **1** and **2** with respect to the 1×2 zone boundary A_2. This is verified by Lorentzian fits about a common symmetry point, which turns out to be A_2 with an uncertainty of 0.01 Å^{-1}.

RELATED CHAIN STRUCTURES

The crystal lattice of Si offers many options for creating step lattices beyond the two sequences discussed so far. The Si(111)5×2-Au structure will be discussed in more detail elsewhere [J. L. McChesney (unpublished)]. Figure 1 shows that apart from terraces separated by single steps there are facets containing multiple steps per unit cell. Many of them produce stable chain structures, such as Si(337)2×1-Au,[20,48–50] Si(5 5 11)-Au,[48–50] Si(225)-Au,[20,33] and Si(110)5×2-Au.[51] Several of them exhibit metallic bands similar to those described in the present study. The most promising of these are listed in Table I.

We find that Si(995)-Au and Si(13 13 7)-Au can be explained in the same scheme as Si(553)-Au. The gold coverages are stoichiometric with a single gold chain per unit cell. Furthermore, their miscut angles are very similar to Si(553) so that all three surfaces can be prepared on the same orientation of silicon wafer simply by changing the gold coverage. We hypothesize that the unit cells of both Si(995)-Au and Si(13 13 7)-Au contain the Si(553)-Au structure as a subunit with the remaining space made up by pure silicon. This model is supported by our measured Fermi surfaces and band structures for Si(13 13 7)-Au (not shown), which are very similar to Si(553)-Au exhibiting both the $\frac{1}{4}$-filled inner band and the $\frac{1}{2}$-filled outer doublet. The fillings of 0.34 and 0.57 are comparable to those for Si(553)-Au. The extra silicon rows do not contribute significantly to the band structure near the Fermi level, which could be explained by the presence of Si adatoms that saturate the extra dangling bonds.

A previous study of Si(337)2×1-Au reported a single metallic band that crosses the Fermi level at the half-filling point $k_F=\pi/2a$.[20] This half-filled band is reminiscent of the nearly half-filled doublet for Si(557)-Au and Si(335)-Au, which are tilted in the same direction.

SUMMARY AND OUTLOOK

In summary, we give an overview of a new class of low-dimensional structures obtained by deposition of gold atoms onto stepped silicon surfaces. They consist of chains of gold atoms and rows of silicon broken bonds in a self-assembled array. Structural models are given that are based on total-energy calculations. Angle-resolved photoemission measurements of these chain structures reveal metallic bands whose Fermi surfaces are nearly one dimensional. It is possible to systematically vary the dimensionality by controlling the spacing of the gold chains via the tilt angle of the substrate from Si(111) and by adjusting the gold coverage accordingly. The two-dimensional versus one-dimensional coupling strengths are measured directly from oscillations around straight Fermi lines, revealing an inverse correlation between the two-dimensional coupling strength and the interchain spacing. The ratios of intrachain to interchain couplings range over an order of magnitude from $t_1/t_2=12$ for Si(553)-Au to $t_1/t_2>100$ for Si(775)-Au.

Apart from the dimensionality there are other characteristics of the electronic structure that can be tailored systematically, most notably the band filling. Bands with a filling from $\frac{1}{4}$-filled to over $\frac{1}{2}$-filled are achieved. The fractional total electron count results from doping of the chains by extra silicon atoms that reside in the two-dimensional unit cell surrounding a one-dimensional chain. Such fractional fillings will be helpful for increasing the electron correlations that produce exotic electronic states while suppressing a Mott-Hubbard transition to an insulator, which occurs in a half-filled band.[11,22] One-quarter-filled bands in other quasi-one-dimensional compounds, such as the Bechgaard salts, have produced strongly correlated Mott states, charge-density-wave phases with spinon and soliton excitations, and hints of Luttinger liquid behavior.[5,52–58] The abundance of gold chain reconstructions on silicon suggests the promise of a large degree of control over the electronic structure, which should make it possible to explore a large region of the electronic phase diagram and to find some of the exotic states predicted for one-dimensional electrons.

ACKNOWLEDGMENTS

Help from A. Kirakosian, J.-L. Lin, and M. Fisher is gratefully acknowledged as well as support from H. H. Weitering. The work was supported by the NSF under Grant Nos. DMR-0240937 and DMR-0079983. It was conducted in part at the Synchrotron Radiation Center, which is supported by the NSF under Grant No. DMR-0084402. Computations were performed at the DOD Major Shared Resource Center at ASC. This work was supported in part by the Office of Naval Research.

[1] J. Solyom, Adv. Phys. **28**, 201 (1979).
[2] K. Schönhammer, in *Strong Interactions in Low Dimensions*, edited by D. Baeriswyl and L. Degiorgi (Klumer Academic, Dordrecht, 2003), Chap. 1, Sec. 5.2.
[3] J. Voit, Rep. Prog. Phys. **58**, 977 (1995).
[4] G. Gruner, *Density Waves in Solids* (Perseus, Cambridge, MA, 1994).
[5] P. M. Chaikin, E. I. Chashechkina, I. J. Lee, and M. J. Naughton, J. Phys.: Condens. Matter **10**, 11 301 (1998).
[6] F. J. Himpsel, Adv. Phys. **32**, 1 (1983).
[7] *Angle-resolved Photoemission*, edited by S. D. Kevan (Elsevier, Amsterdam, 1992).
[8] R. Losio, K. N. Altmann, and F. J. Himpsel, Phys. Rev. B **61**, 10845 (2000).
[9] J. N. Crain, K. N. Altmann, C. Bromberger, and F. J. Himpsel, Phys. Rev. B **66**, 205302 (2002).
[10] R. Losio, K. N. Altmann, and F. J. Himpsel, Phys. Rev. Lett. **85**, 808 (2000).
[11] J. N. Crain, A. Kirakosian, K. N. Altmann, C. Bromberger, S. C. Erwin, J. L. McChesney, J. L. Lin, and F. J. Himpsel, Phys. Rev. Lett. **90**, 176805 (2003).
[12] F. J. Himpsel, K. N. Altmann, R. Bennewitz, J. N. Crain, A. Kirakosian, J. L. Lin, and J. L. McChesney, J. Phys.: Condens. Matter **13**, 11097 (2001).

[13] A. A. Baski, S. C. Erwin, and L. J. Whitman, Surf. Sci. **392**, 69 (1997).
[14] K. N. Altmann, J. N. Crain, A. Kirakosian, J.-L. Lin, D. Y. Petrovykh, F. J. Himpsel, and R. Losio, Phys. Rev. B **64**, 035406 (2001).
[15] R. Losio, K. N. Altmann, A. Kirakosian, J.-L. Lin, D. Y. Petrovykh, and F. J. Himpsel, Phys. Rev. Lett. **86**, 4632 (2001).
[16] D. Sanchez-Portal, J. D. Gale, A. Garcia, and R. M. Martin, Phys. Rev. B **65**, 081401 (2002).
[17] R. Zdyb, M. Strozak, and M. Jalochowski, Vacuum **63**, 107 (2001).
[18] I. K. Robinson, P. A. Bennett, and F. J. Himpsel, Phys. Rev. Lett. **88**, 096104 (2002).
[19] P. Segovia, D. Purdie, M. Hengsberger, and Y. Baer, Nature (London) **402**, 504 (1999).
[20] S. S. Lee, N. D. Kim, C. G. Hwang, H. J. Song, and J. W. Chung, Phys. Rev. B **66**, 115317 (2002).
[21] J. R. Ahn, H. W. Yeom, H. S. Yoon, and I.-W. Lyo, Phys. Rev. Lett. **91**, 196403 (2003).
[22] R. Claessen, M. Sing, Schwingenschlogl, P. Blaha, M. Dressel, and C. S. Jacobsen, Phys. Rev. Lett. **88**, 096402 (2002).
[23] A. Kirakosian, R. Bennewitz, F. J. Himpsel, and L. W. Bruch, Phys. Rev. B **67**, 205412 (2003).
[24] R. Bennewitz, J. N. Crain, A. Kirakosian, J.-L. Lin, J. L. McChesney, D. Y. Petrovykh, and F. J. Himpsel, Nanotechnology **13**, 499 (2002).
[25] J. Kuntze, A. Mugarza, and J. E. Ortega, Appl. Phys. Lett. **81**, 2463 (2002).
[26] S. C. Erwin and H. H. Weitering, Phys. Rev. Lett. **81**, 2296 (1998).
[27] D. Y. Petrovykh, K. N. Altmann, J.-L. Lin, F. J. Himpsel, and F. M. Leibsle, Surf. Sci. **512**, 269 (2002).
[28] A. Kirakosian, J. L. McChesney, R. Bennewitz, J. N. Crain, J. L. Lin, and F. J. Himpsel, Surf. Sci. **498**, L109 (2002).
[29] F. J. Himpsel, A. Kirakosian, J. N. Crain, J. L. Lin, and D. Y. Petrovykh, Solid State Commun. **117**, 149 (2001).
[30] F. J. Himpsel, T. Jung, A. Kirakosian, J. L. Lin, D. Y. Petrovykh, H. Rauscher, and J. Viernow, MRS Bull. **24**, 20 (1999).
[31] J. Viernow, J. L. Lin, D. Y. Petrovykh, F. M. Leibsle, F. K. Men, and F. J. Himpsel, Appl. Phys. Lett. **72**, 948 (1998).
[32] E. Bauer, Surf. Sci. **250**, L379 (1991).
[33] N. Kurahashi, H. Minoda, Y. Tanishiro, and K. Yagi, Surf. Sci. **438**, 91 (1999).
[34] S. C. Erwin (unpublished).
[35] G. Kresse and J. Hafner, Phys. Rev. B **47**, 558 (1993).
[36] G. Kresse and J. Furthmuller, Phys. Rev. B **54**, 11 169 (1996).
[37] D. Sanchez-Portal and R. M. Martin, Surf. Sci. **532**, 655 (2003).
[38] S. C. Erwin, Phys. Rev. Lett. **91**, 206101 (2003).
[39] K. C. Pandey, Phys. Rev. Lett. **49**, 223 (1982).
[40] A. Kirakosian, R. Bennewitz, J. N. Crain, T. Fauster, J. L. Lin, D. Y. Petrovykh, and F. J. Himpsel, Appl. Phys. Lett. **79**, 1608 (2001).
[41] M. Jalochowski, M. Strozak, and R. Zdyb, Surf. Sci. **375**, 203 (1997).
[42] F. J. Himpsel, G. Hollinger, and R. A. Pollak, Phys. Rev. B **28**, 7014 (1983).
[43] At low temperatures where the photovoltage saturates at the *p*- and *n*-type Schottky barriers, the Fermi level position in the gap can be determined by comparing Si 2*p* core-level positions for *p*- and *n*-type samples.
[44] N. W. Ashcroft and N. D. Mermin, *Solid State Physics* (Saunders College Publishing, Philadelphia, 1976).
[45] J. N. Crain (unpublished).
[46] K. B. Blagoev and K. W. Bedell, Phys. Rev. Lett. **79**, 1106 (1997).
[47] R. Plass and L. D. Marks, Surf. Sci. **380**, 497 (1997).
[48] A. A. Baski, K. M. Jones, and K. M. Saoud, Ultramicroscopy **86**, 23 (2001).
[49] A. A. Baski and K. M. Saoud, J. Cluster Sci. **12**, 527 (2001).
[50] A. A. Baski, K. M. Saoud, and K. M. Jones, Appl. Surf. Sci. **182**, 216 (2001).
[51] J. L. McChesney, J. N. Crain, F. C. Zhang, R. Bennewitz, and F. J. Himpsel (unpublished).
[52] F. Zwick, S. Brown, G. Margaritondo, C. Merlic, M. Onellion, J. Voit, and M. Grioni, Phys. Rev. Lett. **79**, 3982 (1997).
[53] F. Mila and K. Penc, Phys. Rev. B **51**, 1997 (1995).
[54] K. Penc and F. Mila, Phys. Rev. B **50**, 11429 (1994).
[55] F. H. L. Essler and A. M. Tsvelik, Phys. Rev. Lett. **88**, 096403 (2002).
[56] D. Poilblanc, G. Montambaux, M. Heritier, and P. Lederer, Phys. Rev. Lett. **58**, 270 (1987).
[57] V. Vescoli, J. Favand, F. Mila, and L. Degiorgi, Eur. Phys. J. B **3**, 149 (1998).
[58] D. G. Clarke, S. P. Strong, P. M. Chaikin, and E. I. Chashechkina, Science **279**, 2071 (1998).